JMEPEG (2021) 30:3884–3891
https://doi.org/10.1007/s11665-021-05696-2

1059-9495/$19.00

Effect of Vanadium on Superhardenability of 23MnNiMoCr54V Steel for Round-Link Chain in Mining Applications

Zhu Zhe, Chen Qiwei, Sun Shuhua, Li Rongbin, Qi Jianjun, Liu Haonan, Lv Zhiqing, and Fu Wantang

Submitted: 10 November 2020 / Revised: 26 February 2021 / Accepted: 10 March 2021 / Published online: 19 April 2021

The effect of vanadium on the hardenability and microstructure of 23MnNiMoCr54V steel was investigated after austenitizing at 950 and 1050 °C by dilatometry and end-quenching Jominy tests, combined with nitrogen removal with aluminum. Electron probe micro-analysis, scanning electron microscopy and transmission electron microscopy techniques were used to characterize the microstructure and existence state of vanadium atoms in the steel. The presence of aluminum-stabilized nitrogen by aluminum nitride production, which promoted the segregation of solid solution vanadium atoms at grain boundaries, delayed the transformation of ferrite and improved the austenite stability. Thus, vanadium addition could improve the hardenability, and an excellent steel performance could be obtained during slower cooling. This process could be used to produce heavy section steel components, such as round-link chains for mining applications.

Keywords aluminium nitride, grain boundary segregation, Jominy test, superhardenability, v-microalloying

1. Introduction

High-strength round-link chains in mining applications are subjected to harsh conditions (Ref 1, 2). Large round-link chain sections are often manufactured to handle combined high load and stress conditions (Ref 3, 4), which increases heat-treatment and processing requirements. Quenching and tempering are required in the final heat treatment to ensure a good hardenability and to meet mechanical standards for the mid-thickness region of the round-link chain. An improvement in the hardenability of large round-link chain steel by adjusting its chemical composition and heat treatment is an important issue for development (Ref 5-7).

Steel hardenability tends to be related to the chemical composition and austenite grain size. Quantitative relationships between hardenability and composition or grain size have been established (Ref 8). However, properties that are inconsistent with these relationships, such as the superhardenability, have been reported (Ref 9). Brown et al. (Ref 10) reported that a significant increase in hardenability was observed after superheating B.S. 970 150M36 melts (similar to SAE 1340) to 1650 °C, and the concept of a superhardening effect was proposed. An excellent hardenability could be achieved through the addition of a certain amount of Al or Ti during smelting and an increase in smelting temperature for common alloyed steels (Ref 11). However, the improvement is difficult to calculate and explain using the alloying element content. Cias et al. (Ref 12) studied the transformation kinetics of superhardened steel and reported that the rate of ferrite nucleation and growth in superhardened steel were inhibited. The pearlite transformation was delayed, and the martensitic transformation was promoted in superhardened steel. Other studies have shown that the acquisition of a superhardenability in steel correlated positively with the fundamental hardenability. A better fundamental hardenability led to a more pronounced superhardenability and a higher ratio between the actual and theoretical hardenability (Ref 13). Therefore, the superhardenability mechanism is related to alloying elements, such as Al, Ti, B, and other alloying elements, which affect the fundamental hardenability.

Alloying element addition, such as V addition, can improve the hardenability, and the amount of V determines if the element acts as an alloying or microalloying addition. Mangonon et al. (Ref 14, 15) and Lagneborg et al. (Ref 16) studied the relationship between V and the hardenability, and reported that the hardenability of V-containing steel was ~1.5 times that in the absence of V. However, other studies have reported that V addition did not improve the hardenability (Ref 17). For example, Garbarz et al. (Ref 17) and Pickering et al. (Ref 18) reported that the rate of ferrite nucleation and growth on grain boundaries could only be inhibited when the microalloying elements existed in solid solution as atoms on the austenite grain boundaries without compound formation. Yoshimura et al. (Ref 19) pointed out that, in high Alγ steels, the γ→α proeutectoid ferrite reaction is retarded through the increase in the incubation period of nucleation and through the decrease in the nucleation rate of ferrite and in the diffusion coefficient of C in austenite. They concluded that the hardenability could only be improved under these conditions. The migration rate of austenitic grain boundaries during reheating affects V segrega-

Zhu Zhe, Chen Qiwei, Liu Haonan, Lv Zhiqing, and **Fu Wantang**, State Key Laboratory of Metastable Materials Science and Technology, Yanshan University, Qinhuangdao 066004, China; **Sun Shuhua**, School of Science, Yanshan University, Qinhuangdao 066004, China; **Li Rongbin**, Shanghai Engineering Research Center of Hot Manufacturing, Shanghai Dianji University, Shanghai 20?306, China; and **Qi Jianjun**, HBIS Group Technology Research Institute, Shijiazhuang 050023, China. Contact e-„mail: wtfu@ysu.edu.cn.

tion, which affects the hardenability of V-containing steel (Ref 20-22).

Various questions require clarification. For example, it must be determined whether a superhardened steel effectiveness can reduce the rate of ferrite nucleation and growth. The relationship between the superhardenability mechanism and the existence state or distribution of V atoms must be established. An understanding is required as to why an excessively high austenitizing temperature results in a reduction in steel superhardenability.

In this work, small amounts of V and Al were added to common round-link chain steel of composition 23MnNiMoCr54. The mechanisms to obtain a superhardenability and the related heat-treatment process were studied. The findings from this work provide technical support to develop heavy section round-link chain steel for applications such as mining.

2. Materials and Methods

The tested steels were 23MnNiMoCr54 and 23MnNiMoCr54V, with chemical compositions as listed in Table 1. The 23MnNiMoCr54V steel was obtained by adding V to the 23MnNiMoCr54 steel, combing N with Al, and it eventually ensuring that V was dissolved into austenite.

The tested steels were melted in a 50 kg vacuum induction furnace under ~5 Pa and ~1500 °C. The cone ingot was forged at ~1200 °C into Φ40 × 700 mm bars. Round bar specimens of Φ25 × 100 mm were prepared by wire cutting and machined into standard samples for Jominy end-quenching tests (hereafter referred to as the Jominy test).

A determinations of the phase transformation points and continuous cooling transformation (CCT) curve was carried out on a L78 RITA dilatometer, where the sample size was Φ3 × 10 mm and the protective gas was helium. The specimens were heated to 950 °C at 10 °C/s, held for 20 min, and cooled to room temperature from 0.1 to 20 °C/s. The sample microhardness was tested using a FM-ARS 9000 microhardness tester. The curve of precipitated AlN versus reheating temperature in the 23MnNiMoCr54V steel was calculated with Thermo-calc software and an upgraded version of TCFE2000. On the basis of the calculation results and previous work (Ref 23), three austenitizing temperatures—880, 950, and 1050 °C—were used in the existence and absence of AlN.

The hardenability was examined in accordance with GB/T 225-2006/ISO 642:1999 (Ref 24), after austenitizing at 950 and 1050 °C, each for 30 min. Hardness values were measured 1.5, 3, 5, 7, 9, 11, 13, and 15 mm from the quenching end, and the subsequent points were at intervals of 5 mm. The average hardness values of three measurements for every point on the end-quenching specimens were selected to indicate the hardenability at a specific temperature. The ideal critical diameters and hardenability multiplying factors of the 23MnNiMoCr54V and 23MnNiMoCr54 steels were calculated from the Jominy test results at 950 and 1050 °C, respectively.

Jominy test samples of the two steels under different austenitizing conditions were machined and then sliced with a wire cutter after the Jominy test. Some slices were treated by mechanical grinding and polishing and were etched with saturated picric acid solution. Microstructures were observed under an Axiover 200MAT optical microscope (OM), and the hardness of each point was tested using a TH501 Rockwell Hardness Tester. The distribution of vanadium atoms was analyzed by electron probe micro-analysis (EPMA) using a Shimazu 1720H apparatus. The microstructures were observed under a Hitachi S-4800 cold field emission scanning electron microscope (SEM) with energy-dispersive spectroscopy (EDS) and transmission electron microscopy (TEM) using a Talos f200x microscope with an accelerating voltage of 200 kV. Thin foils were prepared using a Gatan precision polishing system in 10% perchloric acid in alcohol at room temperature after being thinned to ~ 30 μm using silicon-carbide paper.

3. Results

3.1 Jominy Curves of both Steels after Austenitization at 950 °C and 1050 °C

Jominy test curves of the 23MnNiMoCr54V and 23MnNiMoCr54 steels that were austenitized at 950 °C for 30 min are shown in Fig. 1. The hardness at the quenching end is consistent between the two steels, and in each case decreases gradually with an increase in distance from the quenched end, which is attributed to the similar C content and same heat-treatment conditions for the 23MnNiMoCr54V and 23MnNi-

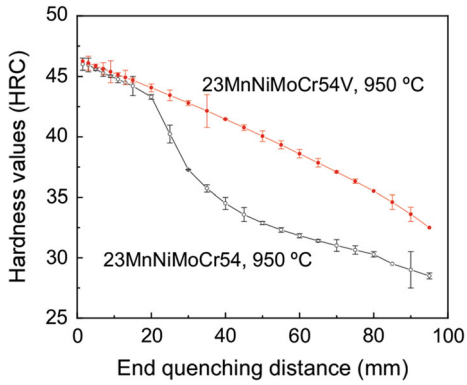

Fig. 1 Jominy test curves of both steels after austenitizing at 950 °C for 30 min

Table 1 Chemical compositions of tested steels (wt.%)

Tested steel	C	V	Si	Mn	Cr	Ni	Mo	Al	N*
23MnNiMoCr54	0.20	…	0.17	1.22	0.49	0.96	0.52	0.026	0.0023
23MnNiMoCr54V	0.22	0.073	0.19	1.29	0.50	0.97	0.54	0.033	0.0022

*N content of steels was remeasured on a nitrogen–oxygen analyzer

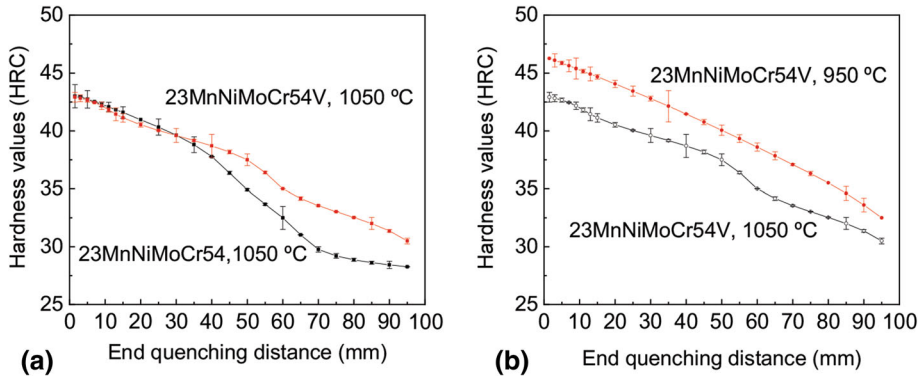

Fig. 2 Jominy test curves for: (a) both steels after austenitizing at 1050 °C and (b) V-containing steel after austenitizing at 950 and 1050 °C

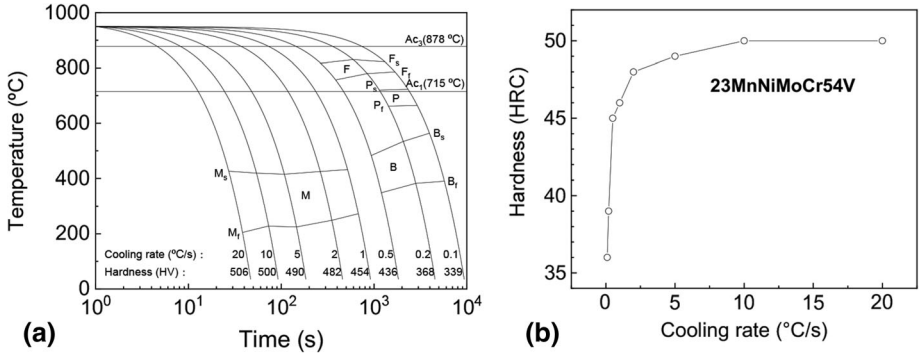

Fig. 3 V-containing steel: (a) CCT curve and (b) microhardness as a function of cooling rate

MoCr54 steels. This result eliminates the possibility that the difference in end-quenching curves results from the different fundamental hardness of the two steels.

A further increase in distance from the quenched end shows a significant hardness difference for the two steels. The 23MnNiMoCr54 steel hardness decreases sharply with an increase in distance from the quenched end when the distance exceeds 20 mm. The hardness decreases to 40 HRC at a distance of 25 mm. In contrast, the hardness of the 23MnNiMoCr54V steel changes slowly with an increase in distance from the quenched end, and it is below 40 HRC at 55 mm from the quenched end. Thus, the 23MnNiMoCr54V steel exhibits a better hardenability than the 23MnNiMoCr54 steel. In general, the austenitizing temperature influences the hardenability significantly. Jominy test curves of 23MnNiMoCr54V and 23MnNiMoCr54 steels after austenitizing at 1050 °C for 30 min are shown in Fig. 2(a), and curves for the 23MnNiMoCr54V steel after austenitizing at 950 and 1050 °C are shown in Fig. 2(b).

Compared with Fig. 1 and 2, the hardenability of the 23MnNiMoCr54V steel that was austenitized at 1050 °C was better than that of the 23MnNiMoCr54 steel, and the hardenability of the 23MnNiMoCr54V steel at 950 °C was better than that at 1050°C. The hardenability difference of the two steels started 20–25 mm from the quenching end for austenitization at 950 °C and 35-40 mm for austenitization at 1050 °C. The maximum hardness difference at the same location from the quenched end after austenitizing at 950 and at 1050 °C was ~7 HRC and 3.5 HRC, respectively. So, it is better austenitizing the V-containing steel at 950 °C.

3.2 CCT Curve and Microstructure of 23MnNiMoCr54V steel

Figure 3 shows the CCT curve and microhardness as a function of cooling rate for the 23MnNiMoCr54V steel that was determined after austenitization at 950 °C for 20 min, aided the results of microstructural examinations. The Ac_1 and Ac_3 of the steel are 715 °C and 878 °C, respectively. When the cooling rate is below 0.2 °C/s (at approximately the cooling for which the microhardness is 368 or lower), the austenite/ferrite + pearlite + bainite transformation can occur, but if the cooling rate exceeds 1.0 °C/s only martensite transformation occurs (Fig. 3a). The Ms point of the steel, which is determined by dilatometry, is 432 °C.

The relationship between steel microhardness and cooling rates is shown in Fig. 3(b). Figure 3(b) shows that the microhardness increases with an increase in cooling rate. When the cooling rate is below 2 °C/s, the microhardness values increases rapidly, but when it exceeds 2 °C/s, the change in microhardness with an increased cooling rate is reduced significantly. The quantitative expression between the hardness (HRC) and the cooling rate (v), after nonlinear fitting, is :

$$\mathrm{HRC} = 50 - 5\exp(-v/3) - 15\exp(-v/0.2) \qquad \text{(Eq 1)}$$

Figure 4 shows the microstructural morphology of the 23MnNiMoCr54V and 23MnNiMoCr54 steels at 5, 25, and 55 mm from the quenched end. At 5 mm from the quenched end, the transformation products correspond to regular lath martensite (Fig. 4 a and d) because the cooling rate reaches and even exceeds the critical cooling rate for martensitic transformation

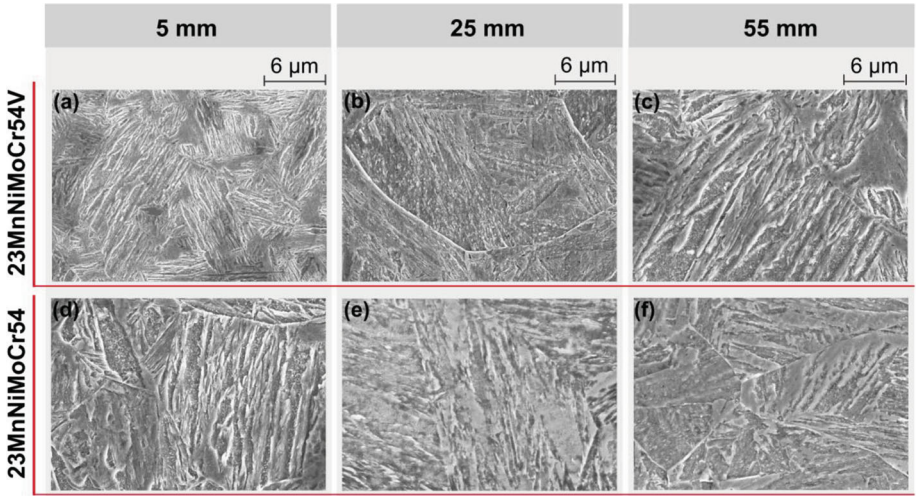

Fig. 4 SEM images of samples from the quenched end for: V-containing steel (a) 5, (b) 25, and (c) 55 mm and 23MnNiMoCr54 steel (d) 5, (e) 25, and (f) 55 mm

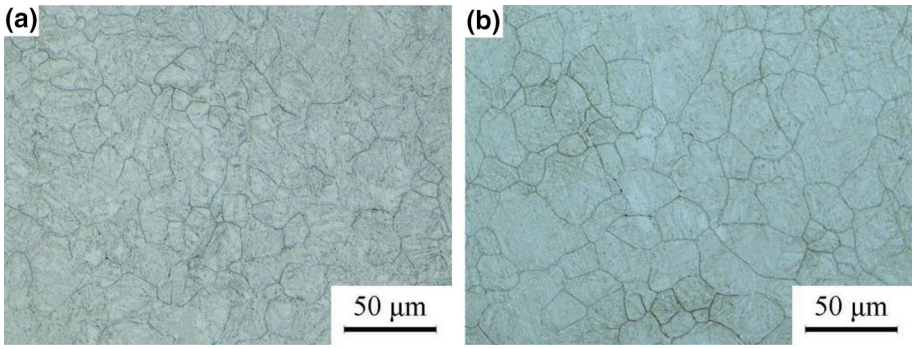

Fig. 5 OM images of original austenite grains for (a) 23MnNiMoCr54 steel and (b) V-containing steel, after Jominy test with austenitizing at 950 °C for 30 min

in the 23MnNiMoCr54V (1.0 °C/s in Fig. 3a) and 23MnNiMoCr54 steels. At 25 mm from the quenched end, although the cooling rate decreases sequentially, complete martensitic transformation still occurs with wider lath martensite in the 23MnNiMoCr54V steel (Fig. 4b), but such a transformation does not in the 23MnNiMoCr54 steel (Fig. 4e). Thus, the growth of featheriness upper bainite occurs from the original grain boundaries as observed in Fig. 4(e). At 55 mm from the quenched end, the cooling rate decreases along the length. The widened lath martensite still increases in the 23MnNiMoCr54V steel (Fig. 4c), but granular bainite in the ferrite matrix is observed in the 23MnNiMoCr54 steel (Fig. 4f). The microstructural results of the two steels in different locations verify the hardness distribution of the Jominy test and show that the 23MnNiMoCr54V steel has a higher hardenability than the 23MnNiMoCr54 steel.

Figure 5 shows the morphology of the original austenite grains of the end-quenched samples after the Jominy test with austenitizing at 950 °C for 30 min. The average grain size of the 23MnNiMoCr54 and 23MnNiMoCr54V steels is ~16 μm (ASTM grain size 8.5–9.0), which shows that the hardenability difference between the two steels is not caused by the difference in austenitic grain size.

4. Discussion

4.1 Superhardenability of 23MnNiMoCr54V steel

The ideal critical diameter (DIV) of the 23MnNiMoCr54V steel can be determined by using end-quenching curves. The hardenability multiplying factor of 23MnNiMoCr54V steel was calculated from the hardenability results at an austenitizing temperature of 950 °C. For steels that contain 0.1%C–0.7%C, the relationship between the hardness of 50% martensite and the C content is (Ref 25, 26):

$$HRC_{50} = 23 + 50 \times \%\,C \qquad \text{(Eq 2)}$$

where HRC_{50} is the hardness of 50% martensite and %C is the mass percentage of C in the steel. The 50% martensite hardness is 34 HRC in the 23MnNiMoCr54V steel and 33 HRC for 23MnNiMoCr54 steel. According to the 50% martensite hardness, the end-quenching distance that corresponds to 34 HRC is 88.07 mm from the water-quenched end in the hardenability curves at 950 °C for the 23MnNiMoCr54V steel. Similarly, the end-quenching distance that corresponds to 33 HRC occurs at 48.50 mm in the 23MnNiMoCr54 steel. On the basis of the relationship between the distance from the quenching end and the ideal critical diame-

ter (DI) (Ref 27), the DI values of the 23MnNiMoCr54V and 23MnNiMoCr54 steels were 335.20 mm and 160.52 mm, respectively. The hardenability multiplying factor of the 23MnNiMoCr54V steel (f) can be calculated as (Ref 28):

$$f = \mathrm{DIV} / \mathrm{DI} = 335.20\ \mathrm{mm}/160.52\ \mathrm{mm} = 2.09 \quad \text{(Eq 3)}$$

The DI of the 23MnNiMoCr54V steel is improved significantly compared with the 23MnNiMoCr54 steel, which indicates that the former has an extremely high hardenability.

Grossmann (Ref 27) suggested that the steel hardenability is related only to the chemical composition and austenite grain size, based upon which the hardenability criterion was established. As a result, the quantitative relationship between the calculated ideal critical diameter (DI'), chemical composition, and grain size is:

$$\mathrm{DI}' = \mathrm{MF_C} \times \mathrm{MF_V} \times \mathrm{MF_{Si}} \times \mathrm{MF_{Mn}} \times \mathrm{MF_{Cr}} \times \mathrm{MF_{Ni}} \times \mathrm{MF_{Mo}} \times \mathrm{MF_{GS}} \quad \text{(Eq 4)}$$

where $\mathrm{MF_{GS}}$ is the multiplication factor of the original austenite gran size, and the other MF parameters are the multiplication factors of the C content and other alloying elements in the steel. Thus, the calculated idea critical diameter (DIV') of the 23MnNiMoCr54V steel is:

$$\begin{aligned}\mathrm{DIV}' &= \mathrm{MF_{CV}} \times \mathrm{MF_{VV}} \times \mathrm{MF_{SiV}} \times \mathrm{MF_{MnV}} \times \mathrm{MF_{CrV}} \times \mathrm{MF_{NiV}} \times \mathrm{MF_{MoV}} \times \mathrm{MF_{GSV}} \\ &= 0.119 \times 1.120 \times 1.133 \times 5.459 \times 2.080 \times 1.352 \times 2.620 \times 0.853 \\ &= 5.18\ \mathrm{in} = 131.57\ \mathrm{mm}.\end{aligned}$$

Mostert et al. (Ref 28) reported that if superhardenability occurs, then the DI of the steel that is obtained from the end-quenching curve deviates from the DI', as predicted by the calculation of chemical composition and grain size. Therefore, a more reasonable superhardenability criterion (superhardenability multiplication factor, SMF) was suggested (Ref 28). The 23MnNiMoCr54V steel SMF is given as:

$$\mathrm{SMF} = \mathrm{DIV}/\mathrm{DIV}' = 335.20\ \mathrm{mm}/131.57\ \mathrm{mm} = 2.55 \quad \text{(Eq 5)}$$

The DI of the 23MnNiMoCr54V steel is ~2.55 times that of the DI'. Thus, the hardenability improvement of the steel exceeds the influence limit of ordinary alloying elements, such as Mn, Ni, Mo, and Cr, so the higher hardenability is related closely to the superhardenability performance of V.

The influence of V on the improvement in hardenability can be calculated by comparing the DI of the 23MnNiMoCr54 and 23MnNiMoCr54V steel and the influencing factors of each alloying element (Ref 29). The hardenability multiplying factor of V (f_{V}) is:

$$\begin{aligned}f_{\mathrm{V}} &= (\mathrm{DI}'/\mathrm{MF_{GS}})/[\mathrm{DIV}'/(\mathrm{MF_{VV}} \times \mathrm{MF_{GSV}})] \times f \\ &= (94.92\ \mathrm{mm}/0.853)/[131.55\ \mathrm{mm}/(1.12 \times 0.853)] \times 2.09 = 1.69.\end{aligned} \quad \text{(Eq 6)}$$

A linear relationship tends to exist for normal steel without superhardenability between the hardenability multiplying factor (f_{V}) and the V content (V) (Ref 30):

$$f_{\mathrm{V}} = 1 + 1.73 \times \mathrm{V} \quad \text{(Eq 7)}$$

where V is the V content in wt.% and 1.73 is the hardenability influencing factor of V. For steel with a superhardenability, the same content of V can yield a more pronounced effect. By replacing 1.73 with z in Eq. (7), i.e., $f_{\mathrm{V}} = 1 + z \times \mathrm{V}$:

$$z = (f_{\mathrm{V}} - 1)/\mathrm{V} = (1.69 - 1)/0.073 = 9.45 \quad \text{(Eq 8)}$$

The larger slope (9.45) shows the significant effects of the superhardenability performance on the steel hardenability, compared with other methods to improve the hardenability (for example, by adding more alloying elements). For the 23MnNiMoCr54V steel, the superhardenability can be obtained by adding a small amount of V and an appropriate amount of Al.

4.2 Mechanism of Superhardenability for 23MnNiMoCr54V Steel

Grobler et al. (Ref 22) reported that an excessively high austenitizing temperature could lead to a loss of superhardenability. A comparison of the Jominy test curves from Fig. 1 and 2 shows that the heat-treatment conditions for quenching can influence the superhardenability performance significantly.

Figure 6 shows a Thermo-calc simulation image of the AlN precipitation curve in the 23MnNiMoCr54V steel. AlN can precipitate only when the heating temperature is below 1021 °C under thermodynamic equilibrium conditions. Hence, it is reasonable to think that if the austenitizing temperature is below 1021 °C, AlN may exist in samples of the Jominy test. Thus, two austenitizing temperatures of 950 and 1050 °C were determined for the heat treatment of Jominy test samples that correspond to the existence and absence of AlN, respectively.

Figure 7 shows a TEM image of the 23MnNiMoCr54V steel after end quenching for different austenitizing temperatures. There is little difference in the shape of the martensitic lath for different austenitizing temperatures, as shown in Fig. 7(a) (950 °C) and b (1050 °C). The effect of austenitizing temperature is shown mainly in the presence of Al and/or V precipitate. No precipitate that contained Al was observed after austenitizing at 1050 °C, but the precipitate particle with a diameter of ~430 nm was observed after austenitizing at 950 °C (Fig. 7c). The composition of the precipitate is shown in Fig. 7d and contains mainly AlN and AlC. No vanadium nitride (VN) was found for austenitizing at 950 °C. Therefore, all V atoms in the steel exist in solid solution (austenite) rather than in compounds, such as VN. As a result, the diffusion or

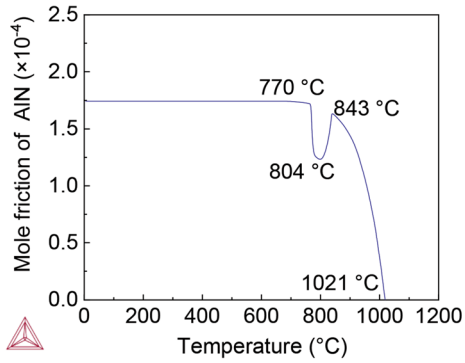

Fig. 6 Thermo-calc simulation image of AlN precipitation curve in V-containing steel

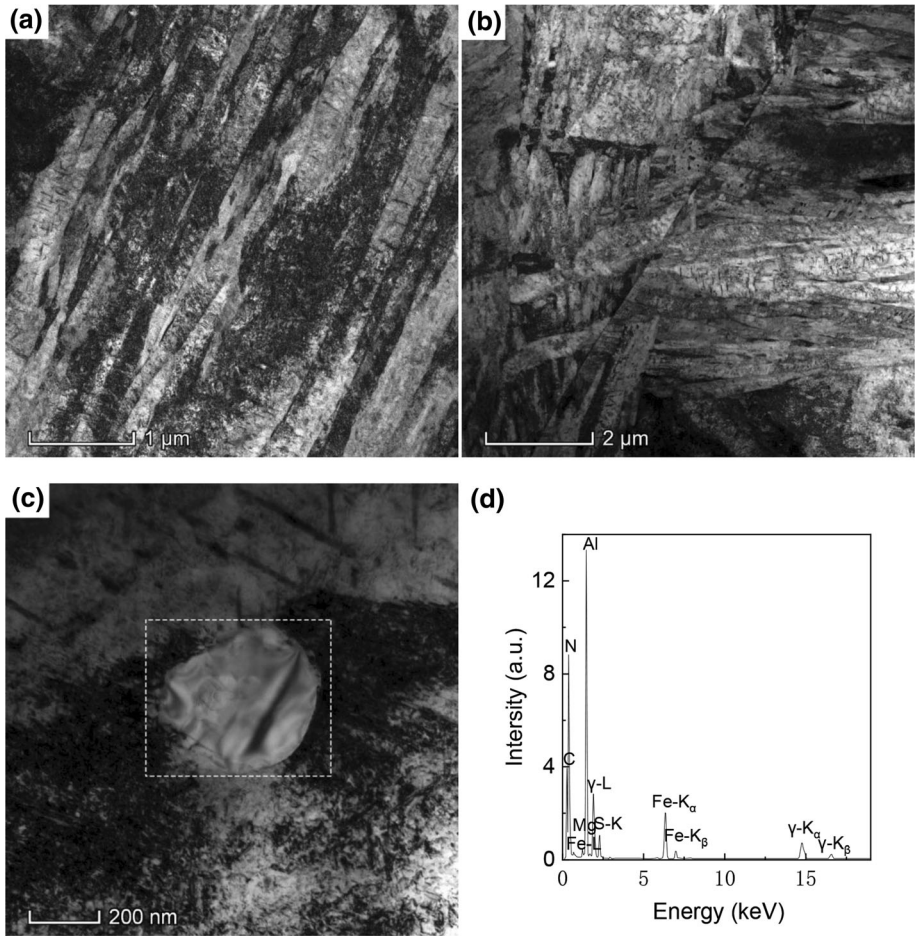

Fig. 7 TEM images of V-containing steel after austenitizing at (a) 950 °C, (b) 1050 °C, (c) 950 °C, and (d) energy spectrum data of precipitates in (c)

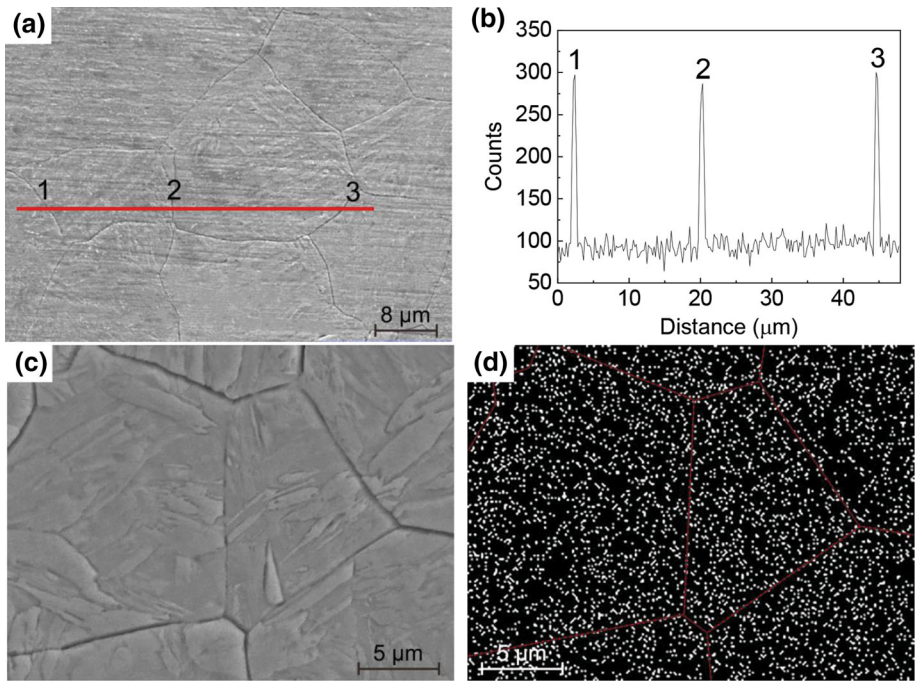

Fig. 8 Grain morphology and result of V distribution in water-quenched sample of V-containing steel after austenitizing at 950 °C for 0.5 h (a and b, EPMA), at 880 °C for 1 h (c and d, EDS with Vk_{α})

segregation of independent V atoms may be easy during austenitizing.

Figure 8 shows the morphology of the original austenite grain boundaries and the corresponding EPMA/EDS result of the V distribution in the water-quenched samples of 23MnNiMoCr54V steel after austenitizing at 950 °C for 0.5 h and at 880 °C for 1 h, respectively. The red line in Fig. 8(a) shows where some original austenitic grain boundaries exist. Figure 8 (a) and (b) show that V segregation in the grain boundaries is much higher than in other parts (intercrystallite) for austenitizing at 950 °C. However, the distribution of V atoms is mainly homogeneous either in grain boundaries or within grains for austenitizing at 880 °C (Fig. 8 c and d). Because the presence and the absence of superhardenability have been exhibited in samples that were austenitized at 950 and 880 °C, respectively, V segregation in the original grain boundaries is required to obtain the superhardenability. This result is consistent with the results of Mostert et al. (Ref 28), and a similar behavior of boron atoms has been used and reported in steels (Ref 30). Therefore, superhardenability in a heavy section round-link chain steel can be achieved through V segregation at austenite grain boundaries, which, in turn, could be achieved by controlling the amounts of alloying elements, such as V, Al, and N, and adjusting the heat-treatment process.

Ferrite in a proeutectoid steel tends to nucleate at the austenitic grain boundary during continuous cooling. When V atoms segregate at the grain boundary and occupy dense defect positions, the fluctuation of energy, composition, and structure required to form the new phase (ferrite) may be inhibited, which impedes ferrite nucleation at the grain boundary. Ferrite growth requires migration of the austenite/ferrite interface. If the defect location is filled, the interfacial energy is reduced and the austenitic grain boundary is stabilized, which reduces the ferrite growth rate. In proeutectoid steel, ferrite is the precursor for pearlite transformation. The formation and increased growth rate of ferrite will hinder pearlite transformation.

In summary, to acquire a superhardenability in V-containing steel, it is necessary to ensure AlN or AlC precipitation during austenitizing, to combine C or N atoms preferentially. With minimal free C and N atoms, most V atoms segregate independently at austenite grain boundaries. The nucleation and growth rates of proeutectoid ferrite are reduced during continuous cooling. Martensitic transformation is promoted and the steel hardenability is improved.

5. Conclusions

The following conclusions can be made:

(1) The addition of moderate amounts of V and Al into 23MnNiMoCr54 steel improved the hardenability. The ideal critical diameter reached 335.20 mm, the hardenability multiplying factor reached 2.09, and the superhardenability multiplication factor reached 2.55 for the V-containing steel.

(2) An excessively high austenitizing temperature led to AlN dissolution, which affected the superhardenability significantly. The most appropriate austenitizing temperature is 950 °C for the V-containing steel.

(3) The acquisition of a superhardenability in 23MnNiMoCr54V steel required that N be stabilized by Al to form AlN and prevent the formation of VN. V segregation at austenite grain boundaries and the occupation of favorable interstitial sites hindered C diffusion, reduced the nucleation and growth rates of proeutectoid ferrite, delayed the transformation of ferrite, and improved the steel hardenability.

Acknowledgments

This work was supported by the Shanghai Engineering Research Center of Hot Manufacturing [No.18DZ2253400] and the Key Research and Development Program of Hebei Province, China [No.20311003D]. We thank Dr. Laura Kuhar, from Liwen Bianji, Edanz Group China (www.liwenbianji.cn/ac), for editing the English text of a draft of this manuscript.

References

1. G. Pantazopoulos, A. Vazdirvanidis, A. Toulfatzis and A. Rikos, Fatigue Failure of Steel Links Operating as Chain Components in a Heavy Duty Draw Bench, *Eng. Failure Anal.*, 2009, **16**(7), p 2440–2449
2. K. Al-Fadhalah, A. Elkholy and M. Majeed, Failure Analysis of Grade-80 Alloy Steel Towing Chain Links, *Eng. Failure Anal.*, 2010, **17**(7–8), p 1542–1550
3. D. Ghosh, S. Dutta, A. K. Shukla, H. Roy, Failure Investigation of a Cage Suspension Gear Chain used in Coal Mines, J. Inst. Eng. (India): Ser. D, 2016, 97, p 255–262
4. S.K. Bhaumik, M. Sujata, M.A. Venkataswamy and M.A. Parameswara, Failure of a Low Pressure Turbine Rotor Blade of an Aeroengine, *Eng. Failure Anal.*, 2006, **13**(8), p 1202–1219
5. R. N. Penha, J. Vatavuk, A. A. Couto, S. A. de L. Pereira, S. A. de Sousa, L. de C. F. Canale, Effect of Chemical Banding on the Local Hardenability in AISI 4340 Steel Bar, Eng. Failure Anal., 2015, 53, p 59–68
6. S. Cao, Y. Kang, X. Zhao and C. Yang, Analysis and Control on Fracture of 20Mn2A High Tensile Steel for Round Link Chain, *J. Iron Steel Res. Int.*, 2011, **18**(S1), p 898–902
7. Z. Wang, J. Qi and Y. Liu, Effect of Silicon Content on the Hardenability and Mechanical Properties of Link-Chain Steel, *J. Mater. Eng. Perform.*, 2019, **28**, p 1678–1684
8. V.B. Nosovi and S.A. Yurasov, Calculation of Hardenability of Structural Steels from their Chemical Composition, *Met. Sci. Heat Treat.*, 1995, **37**, p 16–21
9. R.A. Grange, Estimating the Hardenability of Carbon Steels, *Metall. Trans.*, 1973, **4**, p 2231–2244
10. G.T. Brown and B.A. James, Superhardening in Medium-Carbon Steel, *Met. Technol. (London)*, 1980, **7**(1), p 261–268
11. K. Shimotori, M. Kawai and H. Tokoro, Effects of Al and Ti on Age-Hardenability of 40Cr-Ni Alloy, *J. Jpn. Inst. Met. Mater.*, 1972, **36**(7), p 685–692
12. W.W. Cias, Phase Transformational Kinetics and Hardenability of Low-Carbon, Boron-Treated Steels, *Metall. Trans.*, 1973, **4**, p 603–614
13. H.B. Aaron and G.R. Kotler, Second Phase Dissolution, *Metall. Trans.*, 1971, **2**, p 393–408
14. P.L. Mangonon, Relative Hardenabilities and Interaction Effects of Mo and V in 4330 Alloy Steel, *Metall. Trans. A*, 1982, **13**, p 319–320
15. P.L. Mangonon, The Heat Treatment of Vanadium-Modified Alloy Steels, *JOM*, 1981, **33**(6), p 18–24
16. R. Lagneborg, T. Siwecki, S. Zajac and B. Hutchinson, Role of Vanadium in Microalloyed Steels, *Scand. J. Metall.*, 1999, **28**(5), p 186–241
17. B. Garbarz and F.B. Pickering, Relationship Between Hardness and Microstructure of Continuously Cooled C-Mn-V, *Mater. Sci. Technol.*, 1986, **2**(11), p 1016–1114

18. F.B. Pickering and B. Garbarz, Strengthening in Pearlite Formed from Thermomechanically Processed Austenite in Vanadium Steels and Implications for Toughness, *Mater. Sci. Technol.*, 1989, **5**(3), p 227–237
19. M. Yoshimura, H. Kobayashi and T. Fukuzumi, 低合金肌焼鋼の焼入性と変態挙動へおよぼ AlとNの影響(Effects of Al and N on Hardenability and Transformation Characteristics of Low Alloy Case Hardening Steels), *Tetsu-to-Hagane*, 1983, **69**(3), p 452–461 (**in Japanese**)
20. A. Brownrigg and G.K. Prior, Hardenability Reduction in VN Microalloyed Eutectoid Steels, *Scripta Mater.*, 2002, **46**(5), p 357–361
21. H. Adrian, A Mechanism for Effect of Vanadium on Hardenability of Medium Carbon Manganese Steel, *Mater. Sci. Technol.*, 1999, **15**(4), p 366–378
22. M.V. Li, D.V. Niebuhr, L.L. Meekisho and D.G. Atteridge, A Computational Model for the Prediction of Steel Hardenability, *Metall. Mater. Trans. B*, 1998, **29**, p 661–672
23. J. Qi, Fundamental research on composition design and manufacture process of super heavy link-chain steels for mining, PhD Dissertation, Qinghuangdao: Yanshan university, 2018, Chapter 3.3, p 37–42(in Chinese)
24. X. Li, Y. Luan, X. Yu, G. Wang, S. Sun, Steel-Hardenability Test by end Quenching(Jominy test), GB/T 225-2006/ISO 642:1999, PRC National Standard, 2006, p 1-11(in Chinese)
25. D.E. Coates, Diffusional growth limitation and hardenability, *Metall. Trans.*, 1973, **4**, p 2313–2325
26. C. Gupta, G.K. Dey, J.K. Chakravartty, D. Srivastav and S. Banerjee, A Study of Bainite Transformation in a New CrMoV Steel Under Continuous Cooling Conditions, *Scripta Mater.*, 2005, **53**(5), p 559–564
27. M. A. Grossmann, Hardenability Calculated from Chemical Composition, Met. Technol.(N. Y.), 1942, 150, p 227–259
28. R.J. Mostert and G.T. Van Rooyen, A Quantitative Assessment of the Hardenability Increase Resulting from a Superhardenability Treatment, *Metall. Trans. A*, 1984, **15**(12), p 2185–2191
29. C. Chen, F.C. Zhang, Z.N. Yang and C.L. Zheng, Superhardenability Behavior of Vanadium in 40CrNiMoV Steel, *Mater. Des.*, 2015, **83**, p 422–430
30. Boron steel, edited by First steel works of Benxi steel company, Part 2, Effect of boron in steels, Beijing: Metallurgical Industry Press, 1977, Chapter 1.3, p 24 (in Chinese)